View metadata, citation and similar papers at core.ac.uk

brought to you by CORE

provided by Queensland University of Technology ePrints Archive

Queensland University of Technology
Brisbane Australia

This is the author's version of a work that was submitted/accepted for publication in the following source:

Wan, Hong-Xia & Mahendran, Mahen
(2015)
Behaviour and strength of hollow flange channel sections under torsion and bending.
Thin-walled Structures, *94*, pp. 612-623.

This file was downloaded from: https://eprints.qut.edu.au/87022/

© Copyright 2015 Elsevier Ltd.

License: Creative Commons: Attribution-Noncommercial-No Derivative Works 4.0

Notice: *Changes introduced as a result of publishing processes such as copy-editing and formatting may not be reflected in this document. For a definitive version of this work, please refer to the published source:*

https://doi.org/10.1016/j.tws.2015.05.013

Behaviour and Strength of Hollow Flange Channel Sections under Torsion and Bending

Hong-Xia Wan[1a] and Mahen Mahendran [*2]

[1]*School of Civil Engineering and Architecture, Wuhan University of Technology, Wuhan 430070, PR China*
[2]*School of Civil Engineering and Built Environment, Queensland University of Technology, Brisbane, QLD 4000, Australia*

Abstract. Hollow flange channel section is a cold-formed high-strength and thin-walled steel section with a unique shape including two rectangular hollow flanges and a slender web. Due to its mono-symmetric characteristics, it will also be subjected to torsion when subjected to transverse loads in practical applications. Past research on steel beams subject to torsion has concentrated on open sections while very few steel design standards give suitable design rules for torsion design. Since the hollow flange channel section is different from conventional open sections, its torsional behaviour remains unknown to researchers. Therefore the elastic behaviour of hollow flange channel sections subject to uniform and non-uniform torsion, and combined torsion and bending was investigated using the solutions of appropriate differential equilibrium equations. The section torsion shear flow, warping normal stress distribution, and section constants including torsion constant and warping constant were obtained. The results were compared with those from finite element analyses that verified the accuracy of analytical solutions. Parametric studies were undertaken for simply supported beams subject to a uniformly distributed torque and a uniformly distributed transverse load applied away from the shear centre. This paper presents the details of this research into the elastic behaviour and strength of hollow flange channel sections subject to torsion and bending and the results.

Keywords: Hollow flange channel sections; Cold-formed steel structures; Torsion; Combined torsion and bending.

∗Corresponding author, Professor, E-mail: m.mahendran@qut.edu.au
[a]Associate Professor, E-mail: wanhongxia@vip.tom.com

1. Introduction

Hollow flange channel (HFC) section is a cold-formed high-strength and thin-walled steel section produced using a patented dual electric resistance welding and automated continuous roll-forming process. It has a unique mono-symmetric channel shape comprising two rectangular hollow flanges and a slender web (see Fig. 1). It can be used as flexural members in residential, commercial and industrial buildings. Many experimental and numerical investigations have been undertaken in the past on HFC flexural members at Queensland University of Technology. These investigations were aimed at determining the member moment capacities when they were subjected to lateral distortional and lateral torsional buckling [1-6], the section moment capacities [7,8] and finally the shear capacities [9-13]. They focused on hollow flange channel sections subject to bending action only, which means that they were subjected to transverse loads applied at the shear centre and that member torsion is precluded.

Due to its mono-symmetric characteristics, hollow flange channel section beams will also be subjected to torsion since the transverse loads are applied away from the shear centre. However, torsion is often ignored because it is commonly thought to occur rarely, and when it occurs, it is considered unimportant. Further, difficulties in predicting the effects of torsion discourage designers from considering torsion. Past research on torsion in steel members has concentrated on open sections, typically cold-formed steel channel sections [14,15] and hot-rolled steel I-sections [16-18]. At the same time very few cold-formed steel design standards provide suitable design rules for steel members subject to torsion. Trahair and Pi [19], Pi and Trahir [20,21] and Trahair and Bradford [22] proposed some design methods for steel members subject to torsion. But their design methods and related equations are mainly based on the analysis of hot-rolled I-section members.

Hollow flange channel section has a unique shape including two closed rectangular flanges and a slender web, and thus is quite different from conventional open sections. Its torsional behaviour remains unknown to researchers and designers until now. Therefore in this research the elastic behaviour and strength of hollow flange channel sections subject to uniform torsion, non-uniform torsion and combined torsion and bending were investigated using differential equilibrium equations. The results were then compared with finite element analysis results. Parametric analyses were undertaken for simply supported beams subject to

both uniformly distributed torques, and uniformly distributed transverse loads applied away from the shear centre. This paper presents the details of this research into the elastic behaviour and strength of hollow flange channel section beams subject to torsional and bending actions.

2. Hollow flange channel sections subject to torsion

The section is in a state of uniform torsion when both the rate of change of the angle of twist and the longitudinal warping deflections are constant along the member. The torque acting at any cross-section is only resisted by the shear stresses distributed around the cross-section. Otherwise, it is in a state of non-uniform torsion where the torque is resisted by additional warping shear stresses in conjunction with the shear stresses due to uniform torsion. Whether a member is in a state of uniform torsion or non-uniform torsion depends on the loading arrangement and the warping restraints. In most practical cases non-uniform torsion is encountered. To understand the torsional behaviour of hollow flange channel sections, uniform torsion is investigated first, followed by the analysis of non-uniform torsion.

2.1. Uniform torsion

Hollow flange channel section has a unique shape including two closed rectangular flanges and a slender web. The uniform shear flow, which is the product of shear stress and wall thickness, could be assumed as q in both closed flanges (see Fig. 2(a)) while the shear flow in the web could be assumed to be zero. To determine the shear flow, the section is cut at points “B” and “C” to make it an imaginary open section (see Fig. 2(b)). There would be relative longitudinal displacements at the cut edge due to the actions of torque and shear flow. These relative longitudinal displacements can be written as Eqs. (1) and (2), respectively.

$$u_H = -\theta'(z)\Omega_1 = -2ab\theta'(z) \tag{1}$$

$$u_q = q \oint \frac{ds}{Gt} = \frac{2q}{Gt}(a+b) \tag{2}$$

where $\theta'(z)$ is the rate of change of the twist angle, Ω_1 is twice the area enclosed by one rectangular flange, G is the shear modulus of elasticity, and $\oint ds$ denotes integration around the periphery of one flange.

The sum of Eqs. (1) and (2) should be zero since there are no relative longitudinal displacements in the section. Thus the shear flow in the hollow flanges is given by Eq. (3). The uniform torque could be subsequently obtained by using Eq. (4), and the section torsion constant is given by Eq. (7).

$$q = \frac{ab\theta' Gt}{(a+b)} \tag{3}$$

$$H = 2\Omega_1 q = \frac{4a^2b^2\theta' Gt}{(a+b)} \tag{4}$$

$$J_{d1} = \frac{H}{G\theta'} = \frac{4a^2b^2t}{(a+b)} \tag{5}$$

$$J_{d2} = \frac{2}{3}ht^3 \tag{6}$$

$$J_d = \frac{4a^2b^2t}{(a+b)} + \frac{2}{3}ht^3 \tag{7}$$

where J_{d2} is the web contribution to the section torsion constant, which is much smaller than J_{d1}. Therefore it could be neglected in Eq. (7).

2.2. Non-uniform torsion

2.2.1. Differential equilibrium equation

For a member in a state of non-uniform torsion, the torque is resisted by additional warping shear stresses in conjunction with the shear stresses due to uniform torsion. The resultant of warping shear stresses is named warping torque while the resultant of shear stresses due to uniform torsion is called uniform torque. The sectional total torque $L(z)$ is the sum of warping and uniform torques. This is given by Eq. (8), which is the differential equilibrium equation for non-uniform torsion of multi-cell section [23].

$$L(z) = GJ_d\theta'(z) - E_1J_{\bar{\omega}}\beta'''(z) \tag{8}$$

where E_1 is the converted modulus of elasticity, given by Eq. (9), $\beta(z)$ is the generalized displacement, the relation between $\beta(z)$ and rotation angle $\theta(z)$ given by Eq. (10), $J_{\bar{\omega}}$ is the principal warping constant, given by Eqs. (12) to (14).

$$E_1 = \frac{E}{1-\mu^2} \approx E \tag{9}$$

$$\beta'(z) = \frac{1}{v}\left[\theta'(z) - \frac{L(z)}{GJ_\rho}\right] \tag{10}$$

$$J_\rho = \int \rho^2(s)\, dF \tag{11}$$

$$J_{\bar{\omega}} = \int \bar{\omega}^2\,(s) dF \tag{12}$$

$$\bar{\omega}(s) = \omega(s) - \frac{\int_0^s \frac{sqds}{Gt}}{\theta'} \tag{13}$$

$$\omega(s) = \int_0^s \rho(s) ds \tag{14}$$

In the above equations, E is Young's modulus of elasticity, μ is Poisson's ratio, $\nu = 1 - J_d/J_\rho$, named warping factor, reflecting the warpage of the section, and J_ρ given by Eq. (11) is named the orientation moment of inertia of the section, in which $\rho(s)$ is the perpendicular distance from the shear centre to the tangent of a point on the *s* axis; $\omega(s)$ is principal fan-shaped area coordinate, $\bar{\omega}(s)$ is generalized principal fan-shaped area coordinate; and $dF = tds$ is integral area.

Using the first derivative of both sides of Eq. (8), and assuming that $L(z)$ is no more than a quadratic polynomial, the differential equilibrium equation can be written as Eq. (15).

$$\theta''''(z) - \left(\frac{k}{l}\right)^2 \theta''(z) = \frac{m(z)\upsilon}{E_1 J_{\bar{\omega}}} \tag{15}$$

where

$$m(z) = -dL(z)/dz \tag{16}$$

$$k/l = \sqrt{\frac{GJ_d\upsilon}{E_1 J_{\bar{\omega}}}} \tag{17}$$

2.2.2. Section constants

To get the fan-shaped area coordinates and the generalized fan-shaped area coordinates, the s-axis coordinate of every point along the section mid-line periphery should be determined. This requires a starting point, and a polar point is also needed for determining the polar radius, that is the perpendicular distance from the polar point to the tangent of a point on the s-axis. These two points are called zero point and polar point for fan-shaped area coordinates, respectively. Obviously, different selections of these two points would give different results. Two special points exist, called zero point and polar point for principal fan-shaped area coordinates, respectively. The former is located at the intersections of symmetrical axes and section midlines while the latter is just the sectional shear centre.

To find the shear centre location, the section is assumed to be cut at "B" and "C", and the point numbers around the section are illustrated in Fig. 3. Due to the section symmetry about x axis, only one half of the section is calculated. The centroid "o" is chosen as a temporary polar point while Point "1" is chosen as s-axis initial point, which is the zero point for fan-shaped area coordinate calculations. The calculation sequences around the section are: $1 \rightarrow 2 \rightarrow 3 \rightarrow 4 \rightarrow 5 \rightarrow 6$. The resulting fan-shaped area and generalized fan-shaped area coordinates denoted as ω_O and $\bar{\omega}_O$ are given by Eqs. (18) and (19), respectively. In Eq. (18), $\rho(s)$ denotes the perpendicular distance from the temporary polar point to the tangent of a point on the s-axis.

$$\omega_O(s) = \int_0^s \rho(s) ds \tag{18}$$

$$\bar{\omega}_O(s) = \omega_O(s) - \frac{\int_0^s \frac{sqds}{Gt}}{\theta'} \tag{19}$$

The shear centre location $A(x_A, y_A)$ can be obtained by Eqs. (20a) and (20b).

$$x_A = x_O + \alpha_x \tag{20a}$$

$$y_A = y_O + \alpha_y \tag{20b}$$

where

$$\alpha_x = J_{\bar{\omega}_{Ox}}/J_x \tag{21a}$$

$$\alpha_y = -J_{\bar{\omega}_{Oy}}/J_y \tag{21b}$$

$$J_{\bar{\omega}_{Ox}} = \int \bar{\omega}_O \, y dF \tag{22a}$$

$$J_{\bar{\omega}_{Oy}} = \int \bar{\omega}_O \, x dF \tag{22b}$$

$$J_x = \int y^2 \, dF \tag{23a}$$

$$J_y = \int x^2 \, dF \tag{23b}$$

The shear centre must be located on a symmetrical axis, that gives $\alpha_y = 0$. At the same time, $x_O = y_O = 0$, so the coordinates of the shear centre can be calculated as follows.

$$x_A = \alpha_x \tag{24a}$$

$$y_A = 0 \tag{24b}$$

After the determination of the shear centre location, the generalized principal fan-shaped area coordinates can be calculated using Eqs. (25) to (27).

$$\bar{\omega}(s) = \bar{\omega}_O(s) + \alpha_y x - \alpha_x y + C \tag{25}$$

$$C = -S_{\bar{\omega}_O}/F \tag{26}$$

$$S_{\bar{\omega}_O} = \int \bar{\omega}_O \, dF \tag{27}$$

where F is the sectional area. Due to the $\bar{\omega}_O$ anti-symmetrical property about *x*-axis, $S_{\bar{\omega}_O} = 0$ and $C = 0$. As mentioned before, $\alpha_y = 0$. Thus Eq. (25) is simplified to Eq. (28).

$$\bar{\omega}(s) = \bar{\omega}_O(s) - \alpha_x y \tag{28}$$

Details of nine hollow flange channel sections chosen in the analyses are listed in Table 1. The results of the shear centre locations and generalized principal fan-shaped area coordinates of these sections are also presented in the same table. Subsequently the principal warping constant $J_{\bar{\omega}}$ and the orientation moment of inertia J_ρ can be obtained by Eqs. (12) and (11), respectively. The obtained principal warping constants of these sections are listed in Table 1. Table 2 presents the torsion constant calculated by Eq. (7), the orientation moment of inertia and the resulting warping factor. It could be seen that the warping factors of these sections are closer to 1.0. This means the warping of hollow flange channel section should be significant, and this property is similar to open sections.

In non-uniform torsion, the warping displacements vary along the span of the member while longitudinal strains and corresponding longitudinal warping normal stresses are induced. These stresses define the bimoment stress resultant given as Eq. (29). The relationship between the warping normal stresses and the bimoment can also be given by Eq. (30). It could be seen that the generalized principal fan-shaped area coordinates actually reflect the warping normal stress distribution in a section, which is illustrated in Fig. 4. The warping normal stresses are anti-symmetric about *x*-axis, so only half the section distribution is given in the figure. It can be concluded that the maximum absolute value belongs to Point “5”, which indicates the maximum longitudinal warping normal stress in a section.

$$B(z) = \int \sigma_{\bar{\omega}}(z,s)\, \bar{\omega}(s) dF \tag{29}$$

$$\sigma_{\bar{\omega}}(z,s) = \frac{B(z)}{J_{\bar{\omega}}} \bar{\omega}(s) \tag{30}$$

2.3. Behaviour and strength of steel members in torsion

Very few steel design standards provide design rules for steel members subject to torsion. Trahair and Pi [19], Pi and Trahair [20,21] and Trahair and Bradford [22] proposed four design methods for steel members subject to torsion, namely, plastic design, first hinge design, first yield design and local buckling design. The first yield design method is adopted in this paper since most cold-formed steel member section capacities are based on first yield principles [24].

2.3.1. The first yield uniform torque and the first yield bimoment

In the first yield design, the member strength is assumed to have been reached when the most heavily strained cross-section starts to yield. Pi and Trahair [20] and Trahair and Pi [19] present the first yield design rules for torsion (Eqs. (31) and (32)).

$$M_u^* \le \phi M_{uy} \tag{31}$$

$$B^* \le \phi B_y \tag{32}$$

where M_u^* is the maximum design uniform torque, B^* is the maximum design bimoment, M_{uy} is the first yield uniform torque, B_y is the first yield bimoment, and ϕ is the capacity factor, equal to 0.9. According to Eq. (4), the first yield uniform torque is reached when the shear stress is equal to the shear yield stress, τ_y, that is,

$$M_{uy} = 2\Omega_1 \tau_y t = 4ab\tau_y t \tag{33}$$

As illustrated in Fig. 4, the maximum warping normal stress should occur at Point “5” in a section, which possesses the maximum generalized principal fan-shaped area coordinate. The first yield bimoment is reached when the warping normal stress at Point “5” is equal to the yield stress f_y, that is,

$$B_y = f_y J_{\bar{\omega}} / \bar{\omega}_5 \tag{34}$$

2.3.2. Torsion strength

In this section simply-supported hollow flange channel section members subject to a uniformly distributed torque along their spans are analysed (see Fig. 5). Nine hollow flange channel sections listed in Table 1 were selected with their spans varying from 2m to 10m. The steel grade is G450, with a yield stress $f_y = 450\text{MPa}$ and a shear yield stress

$\tau_y = 270\text{MPa}$.

As described in the previous section, the differential torsion equilibrium equation can be written as Eq. (15), in which m is a constant for a uniformly distributed torque action. This equation can be resolved by using the initial parameter method [23] described in Appendix B. The values of $\theta(z), \theta'(z), B(z)$ and $L(z)$ at any cross-section can be obtained, they are given by Eqs. (B.27), (B.28), (B.29) and (B.30) respectively. The maximum uniform torque occurs at the beam ends while the maximum bimoment occurs at the beam mid-span. The design uniform torque and the design bimoment can be written as Eqs. (35) and (36), respectively.

$$M_u^* = GJ_d\theta'(0) = \frac{ml}{2}\left[1 + \frac{2(1-chk)}{kshk}\upsilon\right] \tag{35}$$

$$B^* = B\left(\frac{l}{2}\right) = \frac{ml^2\upsilon}{k^2}\left[1 - ch\frac{k}{2} + sh\frac{k}{2}\cdot\frac{(chk-1)}{shk}\right] \tag{36}$$

According to the first yield design method, Eqs. (31) and (32) should be satisfied simultaneously, and the maximum design value m^* of uniform distributed torque action and design torsion capacity $M_t = m^*l/2$ are obtained when these two equations are just satisfied. The obtained design torsion capacities for nine hollow flange channel sections with span varying from 2m to 10m are shown in Fig. 6. It is seen that the torsion capacities of the sections with the same flanges are close to each other, and their differences become negligible with increasing span. This could be seen for the first three sections, with dimensions 300×75×25×3.0, 250×75×25×3.0 and 200×75×25×3.0, for Sections 6 and 7 with dimensions 300×60×20×2.0 and 200×60×20×2.0, and also for Sections 8 and 9 with dimensions 200×45×15×2.0 and 150×45×15×2.0. It is concluded that for the same flange size greater section depth contributes little torsion capacity increases, especially for long span members. On the contrary, for the same section depth, greater flange size could improve the torsion capacity significantly. This can be confirmed by Sections 1 and 4 with dimensions $300\times75\times25\times3.0$ and $300\times60\times20\times3.0$, and by Sections 7 and 8 with dimensions 200×60×20×2.0 and 200×45×15×2.0. Fig. 6 also demonstrates that for the same section depth and flange size, the effect of wall thickness is obvious. This is observed for Sections 4, 5 and 6 with dimensions 300×60×20×3.0, 300×60×20×2.5 and 300×60×20×2.0. This proves that increasing thickness will contribute considerably to torsion strength.

3. Finite element analyses of hollow flange channel sections subject to torsion

3.1. Finite element model description

To verify the accuracy of the proposed equations and calculations in the last section, ANSYS 13.0 was used to conduct finite element analyses (FEA) of simply-supported hollow flange channel section members subject to a uniformly distributed torque. The beam element in ANSYS called BEAM189 was used to develop the model. The BEAM189 element is suitable for analysing slender to moderately thick beam structures. The element is a quadratic three-node beam element in 3-D, and provides options for unrestrained warping and restrained warping of cross-sections. With default settings, six degrees of freedom occur at each node including translations in *x*, *y*, and *z* axes and rotations about *x*, *y*, and *z* axes. An optional seventh degree of freedom (warping magnitude) is also available. The element is well-suited for linear, large rotation, and/or large-strain nonlinear applications.

The hollow flange channel section was built by reading a user-defined section mesh in ANSYS. The section was meshed into 32 cells, as illustrated in Fig. 7(a). The beam model was meshed differently into 20 to 100 elements for 2m to 10m span beams. Fig. 7(b) illustrates the typical beam model with 2m span. The warping degree at each node was activated, which means there are seven degrees at each node. One end of the beam was fixed against *x*, *y*, *z* translations and rotation about *x*-axis while the other end was fixed against *y*, *z* translations and rotation about *x*-axis. A uniformly distributed torque of $1\mathrm{N}\cdot\mathrm{m/m}$ was applied, which was uniformly distributed at the element nodes along the beam model. A linear elastic material model was considered, with Young's modulus of elasticity $E = 200\mathrm{GPa}$ and Poisson's ratio $\mu = 0.3$.

3.2. Validation of the finite element model

To validate the developed finite element model, simply-supported cold-formed lipped channel section members subject to a uniformly distributed torque were also analysed. Two cold-formed lipped channel sections reported in [25] were used in these analyses. Table 3 shows the dimensions of these two sections. Fig. 8(a) shows the section cells of the lipped channel section, while Fig. 8(b) shows the beam model. The boundary conditions, load

distributions and material model are the same as those of hollow flange channel sections described earlier. Fig. 9 shows the twisting of lipped channel section after loading. The cross-sectional properties of the two cold-formed channel sections given by FEA are presented in Table 4. Put et al.'s [25] results obtained from THIN-WALL are also presented in this table. A good agreement between the two sets of results indicates that the developed finite element models are reliable.

Yu and LaBoube [26] summarized torsional analysis methods for open cold-formed sections. They include the equations from [27] for the angle of rotation for beams with pinned ends. The angle of rotation for open section beams subject to a uniformly distributed torque is given by Eq. (37), in which $= \sqrt{GJ/EI_\omega}$, and the bimoment is given by Eq. (38).

$$\theta(z) = \frac{m}{GJ\lambda^2}\left[\frac{\lambda^2 l^2}{2}\left(\frac{z}{l} - \frac{z^2}{l^2}\right) + ch\lambda z - th\frac{\lambda l}{2}sh\lambda z - 1\right] \quad (37)$$

$$B(z) = -EI_\omega \theta''(z) \quad (38)$$

The maximum angle of rotation $\theta(l/2)$ and the maximum bimoment $B(l/2)$ at mid-span as m=1 were obtained from the above equations and are compared with the corresponding FEA results in Table 5 for the two cold-formed channel sections with three different spans, 1m, 2m and 3m. It can be seen that the FEA results agree very well with the predictions from the above equations. This demonstrates that the boundary conditions and load distributions in the developed finite element model are appropriate.

3.3. Comparison of FEA results with theoretical results

The validated finite element model was used to conduct the analyses of the nine hollow flange channel sections listed in Table 1, with their spans varying from 2m to 10m. All the analysis processes were implemented by ANSYS command lines. The torsion constant, the shear centre and the principal warping constant given by FEA were compared with the corresponding results obtained by the proposed equations in the last section. Table 6 presents these results including the ratios of the results. It can be seen that the results obtained from the proposed equations are very close to those given by FEA. This demonstrates the accuracy of the proposed calculation methods and equations in Sections 2.1 and 2.2 for uniform and non-uniform torsion of hollow flange channel sections.

Fig. 10 illustrates the twisting of Section 1 with 2m span, for which the maximum angle of twist occurs at mid-span (0.147E-04 rad). The results obtained by Eq. (B.27) as *m*=1 and *z=l/2* is 0.153E-4 rad, which gives a ratio of 1.041. The comparisons of mid-span twist angles for Sections 1, 4, 7 and 8 subject to a uniformly distributed torque of $1\mathrm{N}\cdot\mathrm{m/m}$ with spans varying from 2m to 10m are given in Fig. 11. It shows that the results from Eq. (B.27) and ANSYS agree well. Noticeable differences in the angle of twist can be seen in Fig. 11 for HFC sections with the same depth due to the difference in flange sizes (compare Sections 1 and 4, and Sections 7 and 8). Fig. 12 illustrates the comparison of mid-span bimoment for Section 1. It shows that the results from Eq. (B.29) as *m*=1 and z=*l*/2 also coincide with the results given by ANSYS. These consistencies prove the accuracy of the proposed calculation formulae provided in Appendix B and those adopted in Section 2.3.

4. Hollow flange channel sections subject to combined bending and torsion

Most commonly, hollow flange channel section beams are subjected to transverse loads applied away from the shear centre, which cause combined bending and torsion action. In this section simply supported beams subject to uniformly distributed transverse loads are analysed with the loads acting on the top flange through the centre of flange width. Since this load application is away from the shear centre, it causes combined bending and torsion (see Fig. 1 3). Nine sections listed in Table 1 with spans varying from 2m to 10m were analysed. The linear interaction equation suggested by Pi and Trahair [21] and Trahair and Pi [19] for member design subject to combined bending and torsion is adopted.

$$\frac{M_x^*}{\phi M_{bx}} + \frac{M_z^*}{\phi M_t} \leq 1 \tag{39}$$

where $M_x^* = ql^2/8$ and $M_z^* = (qe)l/2$ are the maximum bending and torsional moments in the member, respectively, *e* is the load eccentricity from the shear centre, ϕM_{bx} is the design moment capacity which includes an appropriate allowance for beam lateral buckling, and ϕM_t is the design torsion capacity for the member when loaded in torsion alone, that is uniformly distributed torque action as discussed in Section 2.3.2. The capacity reduction factor ϕ is suggested to be taken as 1.0 if the maximum bending moment and the maximum torsional moment occur at different cross-sections along the member.

According to the Australian cold-formed steel structures standard AS/NZS 4600 [24], the

bending moment capacity is calculated as follows.

$$M_{bx} = Z_c f_c \tag{40}$$

where $f_c = M_c/Z_f$, M_c is the critical moment, Z_f is the full unreduced section modulus for the extreme compression fibre, and Z_c is the effective section modulus calculated at a stress f_c in the extreme compression fibre. The critical moment shall be calculated as follows.

For $\lambda_b \leq 0.60$: $M_c = M_y$ (41a)

For $0.60 < \lambda_b < 1.336$: $M_c = 1.11 M_y \left[1 - \left(\frac{10\lambda_b^2}{36}\right)\right]$ (41b)

For $\lambda_b \geq 1.336$: $M_c = M_y \left(\frac{1}{\lambda_b^2}\right)$ (41c)

where $\lambda_b = \sqrt{M_y/M_o}$ is the non-dimensional slenderness ratio, $M_y = Z_f f_y$ is the moment causing initial yield in the extreme compression fibre of the full section. M_o is the elastic buckling moment, determined as follows.

$$M_o = C_b \sqrt{\frac{\pi^2 E I_y}{l^2}\left(G J_d + \frac{\pi^2 E J_{\bar{\omega}}}{l^2}\right)} \tag{42}$$

$$C_b = \frac{12.5 M_{max}}{2.5 M_{max} + 3M_3 + 4M_4 + 3M_5} \tag{43}$$

where M_3, M_4, M_5 are the absolute values of the moments at the quarter point, mid-point and three-quarter point of the unbraced segment and M_{max} is the absolute value of the maximum moment.

The maximum design value q^* for the uniformly distributed transverse load is obtained when Eq. (39) is satisfied. Effects of section depth, wall thickness, and flange size on the load carrying capacity of hollow flange channel beams are illustrated by Figures 14(a) to (c) for spans varying from 2m to 10m. As illustrated in Figures 14(a) and (b), greater section depth and thickness contribute to higher load carrying capacity, but the contribution decreases gradually with increasing span. The two figures show that for long span members, increasing the section depth and thickness does not help much in increasing the load carrying capacity. Fig. 14(c) demonstrates that greater flange size could improve the load carrying capacity significantly. Despite the higher depth HFC section 300×60×20×3.0 has similar maximum design load capacity in comparison with HFC section 200×75×25×3.0. This implies that flange size is more influential than section depth for HFC sections subject to torsion and

bending.

Figures 15(a) to (c) show the ratio of M_x^*/M_{bx} for hollow flange channel sections with varying depths and flange sizes. It could be seen in these figures that sections with lower depths and smaller flange sizes possess higher ratios of M_x^*/M_{bx} , ie. achieve greater percentage of their design moment capacities. This ratio is approaching 1.0 with increasing spans, which means long span members are more likely to achieve their design moment capacities. These figures show that flange sizes have a greater influence for longer span members. They also show that torsion reduces the bending strength significantly, especially for short span beams. Long span beams are likely to achieve their design moment capacities.

5. Conclusions

This paper has described the details of an investigation into the elastic behaviour and strength of a cold-formed hollow flange channel section subject to torsion and bending. Elastic analysis was conducted based on the solution of appropriate differential equilibrium equations. Analytical methods for hollow flange channel sections subject to uniform and non-uniform torsion are described in this paper. The results of section shear flow distribution and torsion constant for uniform torsion, and the outcomes of section warping normal stress distribution and warping constant due to non-uniform torsion have both been presented here. These results agreed well with those obtained from finite element analyses using ANSYS and thus confirmed the accuracy of analytical solutions. Based on the first yield design method, parametric studies were then undertaken for simply supported hollow flange channel section members subject to torsion and combined torsion and bending.

For hollow flange channel sections subject to torsion, the results from this study showed that greater flange size and thickness could improve their torsion capacities significantly. However, greater section depth provides limited contribution to torsion capacity increases, especially for long span members. For hollow flange channel sections subject to combined bending and torsion, similar results are obtained for the effects of section depth and flange size on the load carrying capacity. Meanwhile, sections with smaller depths or flange sizes are able to achieve their design moment capacities more easily. Torsion reduces bending strength significantly, especially for short span beams. Beams with long spans are more likely to achieve their design moment capacities. Besides the significant effect on the load carrying

capacity, flange also obviously affects the member's ability to reach its design moment capacity.

Acknowledgements

The authors would like to thank the Queensland University of Technology for providing the necessary research facilities and support to conduct this research project, and China Scholarship Council for funding the first author's overseas research program.

References

[1] Kurniawan CW and Mahendran M. Elastic lateral buckling of simply supported LiteSteel beams subject to transverse loading. Thin-Walled Structures 2009; 47:109-119.

[2] Anapayan T, Mahendran M and Mahaarachchi D. Lateral distortional buckling tests of a new hollow flange channel beam. Thin-Walled Structures 2011; 49:13-25.

[3] Anapayan T and Mahendran M. Numerical modelling and design of LiteSteel Beams subject to lateral buckling. Journal of Constructional Steel Research 2012;70:51-64.

[4] Anapayan T and Mahendran M. Improved design rules for hollow flange channel sections subject to lateral distortional buckling. Thin-Walled Structures 2012;50:128-140.

[5] Seo JK, Mahendran M and Paik JK. Numerical method for predicting the elastic lateral distortional buckling moment of a mono-symmetric beam with web openings. Thin-Walled Structures 2011; 49:713-723.

[6] Seo JK and Mahendran M. Member moment capacities of mono-symmetric LiteSteel Beam floor joists with web openings. Journal of Constructional Steel Research 2012; 70:153-166.

[7] Anapayan T, Mahendran M and Mahaarachchi D. Section moment capacity tests of LiteSteel beams. Thin-Walled Structures 2011; 49:502-512.

[8] Seo JK and Mahendran M. Plastic bending behaviour and section moment capacities of mono-symmetric LiteSteel beams with web openings. Thin-Walled Structures 2011; 49:513-522.

[9] Keerthan P and Mahendran M. Elastic shear buckling characteristics of LiteSteel beams. Journal of Constructional Steel Research 2010; 66:1309-1319.

[10] Keerthan P and Mahendran M. Experimental studies on the shear behaviour and strength of LiteSteel beams. Engineering Structures 2010;32:3235-3247.

[11] Keerthan P and Mahendran M. New design rules for the shear strength of LiteSteel

beams. Journal of Constructional Steel Research 2011;67:1050-1063.

[12] Keerthan P and Mahendran M. Numerical modeling of LiteSteel beams subject to shear. Journal of Structural Engineering 2011;137:1428-1439.

[13] Keerthan P and Mahendran M. Shear Behaviour and Strength of LiteSteel Beams with Web Openings. Advances in Structural Engineering 2012; 15:171-184.

[14] Put BM, Pi YL and Trahair NS. Bending and torsion of cold-formed channel beams. Journal of Structural Engineering 1999;125:540-546.

[15] Gotluru BP, Schafer BW and Pekoz T. Torsion in thin-walled cold-formed steel beams. Thin-Walled Structures 2000; 37:127–145.

[16] Pi YL and Trahair NS. Inelastic bending and torsion of steel I-beams. Journal of Structural Engineering 1994;120:3397-3417.

[17] Pi YL and Trahair NS. Inelastic torsion of steel I-beams. Journal of Structural Engineering 1995;121:609-620.

[18] Pi YL and Trahair NS. Plastic-collapse analysis of torsion. Journal of Structural Engineering 1995; 121:1389-1395.

[19] Trahair NS and Pi YL. Torsion, bending and buckling of steel beams. Engineering Structures 1997;19:372-377.

[20] Pi YL and Trahair NS. Torsion design of steel members. Australian Civil Engineering Transactions 1994; CE36(4):319-324.

[21] Pi YL and Trahair NS. Steel member design for combined torsion and bending. Australian Civil Engineering Transactions 1994; CE36(4):325-330.

[22] Trahair NS and Bradford MA. (1998) The behaviour and design of steel structures to AS4100. Third edition-Australian. London (UK):E&FN Spon; 1998.

[23] Bao SH and Zhou J. Structural mechanics of thin-walled members. Beijing, China: China Building Industry Press; 2006.

[24] Standards Australia, AS/NZS 4600. Cold-formed steel structures. Sydney, Australia; 2005.

[25] Put BM, Pi YL and Trahair NS. Lateral buckling tests on cold-formed channel beams. Journal of Structural Engineering 1999;125:532-539.

[26] Yu W-W, LaBoube RA. Cold-formed steel design. 4th edition. New Jersey, USA: John Wiley & Sons, Inc; 2010.

[27] American Institute of Steel Construction. Torsional analysis of steel members. Chicago, IL, 1983.

Appendix A. Nomenclature

a flange depth(centre line dimension) b flange width(centre line dimension)

h one half of web depth t wall thickness

$O(x_O, y_O)$ centroid $A(x_A, y_A)$ shear centre

q shear flow in flange due to uniform torsion $\theta(z)$ angle of twist

$\theta'(z)$ rate of change of angle of twist Ω_1 twice the area enclosed by one flange

s axis along the section middle line G shear modulus of elasticity

E Young's modulus of elasticity E_1 converted modulus of elasticity

μ Poisson's ratio H uniform torque

J_d torsion constant $\beta(z)$ generalized displacement

$\omega(s)$ principal fan-shaped area coordinate

$\bar{\omega}(s)$ generalized principal fan-shaped area coordinate

$\omega_O(s)$ fan-shaped area coordinate $\bar{\omega}_O(s)$ generalized fan-shaped area coordinate

$J_{\bar{\omega}}$ principal warping constant $dF = tds$ integral area

x, y, z principal axes F sectional area

$\rho(s)$ perpendicular distance from polar point to the tangent of a point on the *s*-axis

$L(Z)$ total torque $B(z)$ bimoment

$\sigma_{\bar{\omega}}(z, s)$ warping normal stress J_x, J_y second moments of area about *x* and *y* axes

J_ρ orientation moment of inertia M_{uy} first yield uniform torque

B_y first yield bimoment M_u^* design uniform torque

B^* design bimoment ϕ capacity factor

f_y yield stress τ_y shear yield stress

M_x^* the maximum bending moment M_z^* the maximum torsion action

ϕM_{bx} design moment capacity ϕM_t design torsion capacity

λ_b non-dimensional slenderness ratio M_y first yield moment

M_o elastic lateral buckling moment

Appendix B. Calculations of $\boldsymbol{\theta(z), \theta'(z), B(z), L(z)}$

For a non-load member segment, the differential equilibrium equation is a homogeneous equation, given by Eq. (B.1), and the solution is Eq. (B.2).

$$\theta''''(z) - \left(\frac{k}{l}\right)^2 \theta''(z) = 0 \tag{B.1}$$

$$\theta(z) = C_1 + C_2 z + C_3 sh\frac{kz}{l} + C_4 ch\frac{kz}{l} \tag{B.2}$$

where $C_i (i = 1,2,3,4)$ are undetermined constants. The relation between the generalized displacement $\beta(z)$ and rotation angle $\theta(z)$ can be given by Eq. (B.3). Substituting Eq. (B.2) into Eq. (B.3), Eq. (B.4) is obtained.

$$\beta'(z) = \frac{1}{v}\left[\theta'(z) - \frac{L(z)}{GJ_\rho}\right] \tag{B.3}$$

$$\beta'(z) = \frac{1}{v}\left[C_2 + C_3\frac{k}{l}ch\frac{kz}{l} + C_4\frac{k}{l}sh\frac{kz}{l} - \frac{1-v}{GJ_d}L(z)\right] \tag{B.4}$$

Because there is no load for the considered member segment, the torque along the segment is unchanged, that is, $L(z) = \text{constant}$ and we get the following equations.

$$B(z) = -E_1 J_{\bar{\omega}}\beta'' = -GJ_d\left(C_3 sh\frac{kz}{l} + C_4 ch\frac{kz}{l}\right) \tag{B.5}$$

$$L(z) = GJ_d\theta' - E_1 J_{\bar{\omega}}\beta''' = GJ_d C_2 \tag{B.6}$$

Assuming at $z = 0$ section, the initial parameters are:

$$\theta(0) = \theta_0, \beta'(0) = \beta_0', B(0) = B_0, L(0) = L_0 \tag{B.7a)-(B.7d}$$

Substituting the above equations into Eqs. (B.2), (B.4), (B.5), and (B.6), respectively, the following results are obtained.

$$\theta_0 = C_1 + C_4 \tag{B.8}$$

$$\beta_0' = \frac{1}{v}\left(C_2 + C_3\frac{k}{l} - \frac{1-v}{GJ_d}L_0\right) \tag{B.9}$$

$$B_0 = -GJ_d C_4 \tag{B.10}$$

$$L_0 = GJ_d C_2 \tag{B.11}$$

Solving the above four equations jointly, the constants $C_i (i = 1,2,3,4)$ are obtained.

$$C_1 = \frac{B_0}{GJ_d} + \theta_0 \tag{B.12}$$

$$C_2 = \frac{L_0}{GJ_d} \tag{B.13}$$

$$C_3 = \frac{vl}{k}\left(\beta_0' - \frac{L_0}{GJ_d}\right) \tag{B.14}$$

$$C_4 = -\frac{B_0}{GJ_d} \tag{B.15}$$

Substituting the constants into Eqs. (B.2), (B.4), (B.5), and (B.6), the displacements and internal forces at any section can be expressed using the initial parameters, which are written as the following matrix equations.

$$\{Z(z)\} = [P(z)]\{Z_0\} \tag{B.16}$$

$$\{Z(z)\} = \left\{\theta(z) \quad \beta'(z) \quad -\frac{B(z)}{GJ_d} \quad \frac{L(z)}{GJ_d}\right\}^T \tag{B.17}$$

$$\{Z_0\} = \left\{\theta_0 \quad \beta_0' \quad -\frac{B_0}{GJ_d} \quad \frac{L_0}{GJ_d}\right\}^T \tag{B.18}$$

$$[P(z)] = \begin{bmatrix} 1 & \frac{lv}{k}sh\frac{kz}{l} & ch\frac{kz}{l} - 1 & z - \frac{lv}{k}sh\frac{kz}{l} \\ 0 & ch\frac{kz}{l} & \frac{k}{vl}sh\frac{kz}{l} & 1 - ch\frac{kz}{l} \\ 0 & \frac{lv}{k}sh\frac{kz}{l} & ch\frac{kz}{l} & -\frac{lv}{k}sh\frac{kz}{l} \\ 0 & 0 & 0 & 1 \end{bmatrix} \tag{B.19}$$

For simple supports, the boundary conditions are as follows.

$$\theta(0) = 0, B(0) = 0 \tag{B.20a)-(B.20b)}$$

$$\theta(l) = 0, B(l) = 0 \tag{B.20c)-(B.20d)}$$

At $z = 0$ section, the initial matrix-vector $\{Z(z)\}$ is

$$\{Z(0)\} = \left\{0 \quad \beta_0' \quad 0 \quad \frac{L_0}{GJ_d}\right\}^T \tag{B.21}$$

For a member subject to a uniformly distributed torque m along the length, the matrix-vector $\{Z(z)\}$ at any section can be written as

$$\{Z(z)\} = [P(z)]\{Z(0)\} - \int_0^z [P(z-w)]\{Z(w)\}dw \tag{B.22}$$

where

$$\{Z(w)\} = \left\{0 \quad 0 \quad 0 \quad \frac{m}{GJ_d}\right\}^T \tag{B.23}$$

The result is

$$\{Z(z)\}=\begin{bmatrix} \frac{lv}{k}sh\frac{kz}{l}\beta_0'+\frac{L_0}{GJ_d}\left(z-\frac{lv}{k}sh\frac{kz}{l}\right)-\frac{m}{GJ_d}\left[\frac{z^2}{2}+\frac{l^2v}{k^2}\left(1-ch\frac{kz}{l}\right)\right] \\ ch\frac{kz}{l}\beta_0'+\frac{L_0}{GJ_d}\left(1-ch\frac{kz}{l}\right)-\frac{m}{GJ_d}\left(z-\frac{lv}{k}sh\frac{kz}{l}\right) \\ \frac{lv}{k}sh\frac{kz}{l}\beta_0'-\frac{L_0}{GJ_d}\frac{lv}{k}sh\frac{kz}{l}-\frac{m}{GJ_d}\frac{l^2v}{k^2}\left(1-ch\frac{kz}{l}\right) \\ \frac{L_0}{GJ_d}-\frac{m}{GJ_d}z \end{bmatrix} \tag{B.24}$$

Substituting Eqs. (B.20c) and (B.20d) into the first and third rows of Eq. (B.24), respectively, the initial parameters are obtained.

$$L_0=\frac{1}{2}ml \tag{B.25}$$

$$\beta_0'=\frac{ml}{2GJ_d}\left[1+\frac{2(1-chk)}{kshk}\right] \tag{B.26}$$

The values of $\theta(z),\theta'(z),B(z)$and $L(z)$ at any section for beams subject to a uniformly distributed torque can be described by the following formulae, in which the initial parameters were obtained from Eqs. (B.25) and (B.26).

$$\theta(z)=\frac{lv}{k}sh\frac{kz}{l}\beta_0'+\frac{L_0}{GJ_d}\left(z-\frac{lv}{k}sh\frac{kz}{l}\right)-\frac{m}{GJ_d}\left[\frac{z^2}{2}+\frac{l^2v}{k^2}\left(1-ch\frac{kz}{l}\right)\right] \tag{B.27}$$

$$\theta'(z)=vch\frac{kz}{l}\beta_0'+\frac{L_0}{GJ_d}\left(1-vch\frac{kz}{l}\right)-\frac{m}{GJ_d}\left(z-\frac{lv}{k}sh\frac{kz}{l}\right) \tag{B.28}$$

$$B(z)=-GJ_d\frac{lv}{k}sh\frac{kz}{l}\beta_0'+L_0\frac{lv}{k}sh\frac{kz}{l}+m\frac{l^2v}{k^2}\left(1-ch\frac{kz}{l}\right) \tag{B.29}$$

$$L(z)=L_0-mz \tag{B.30}$$

Fig. 1 Hollow flange channel sections and applications

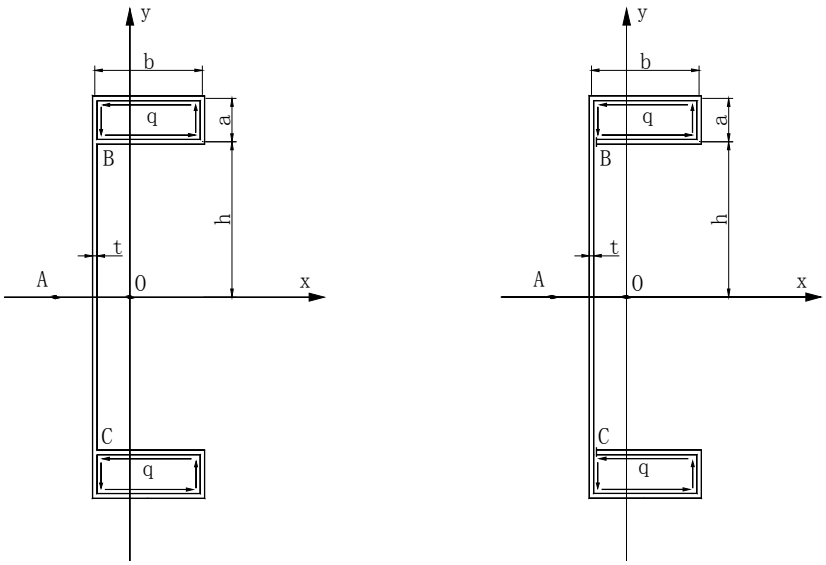

(a) Shear flow distribution (b) Imaginary open section

Fig. 2 Shear flow in hollow flange channel sections

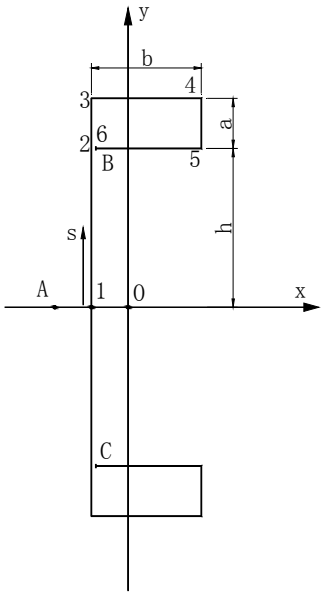

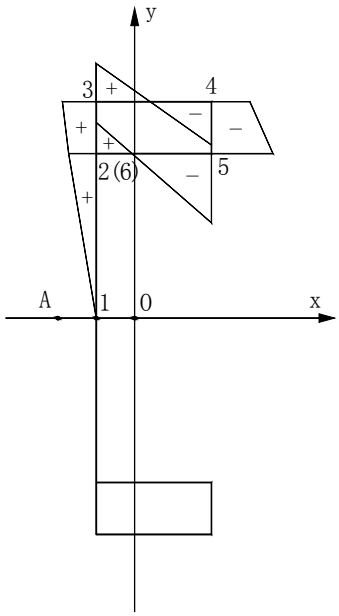

Fig. 3 Illustration of calculation sequences **Fig. 4 Warping normal stress distribution**

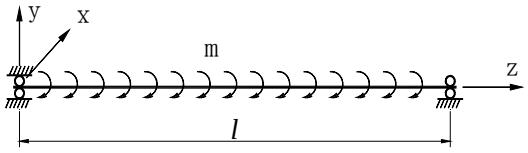

Fig. 5 Illustration of torque distribution

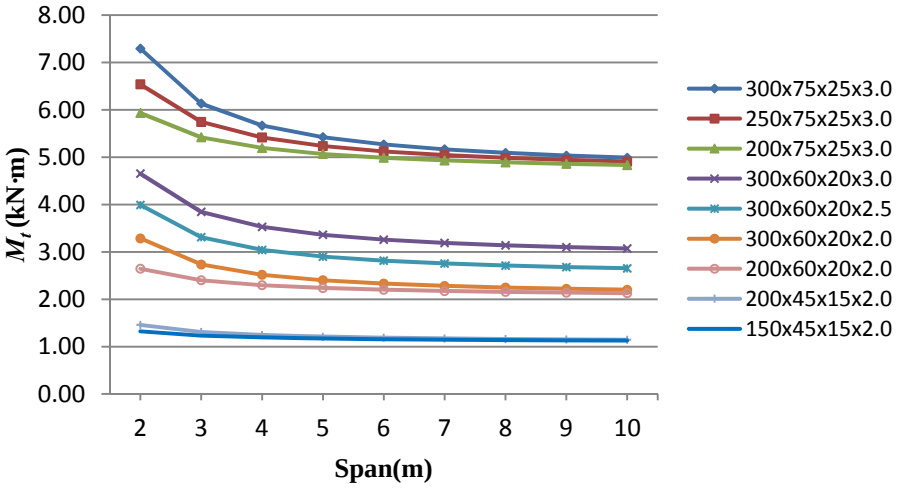

Fig. 6 Torsion capacities of hollow flange channel sections

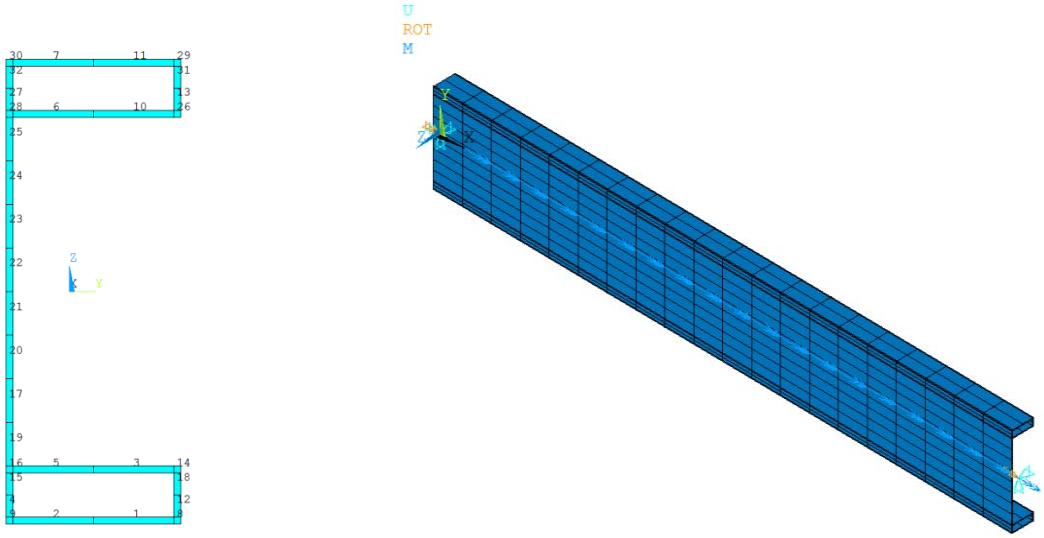

(a) Section cells (b) Beam model

Fig. 7 Finite element model of hollow flange channel section

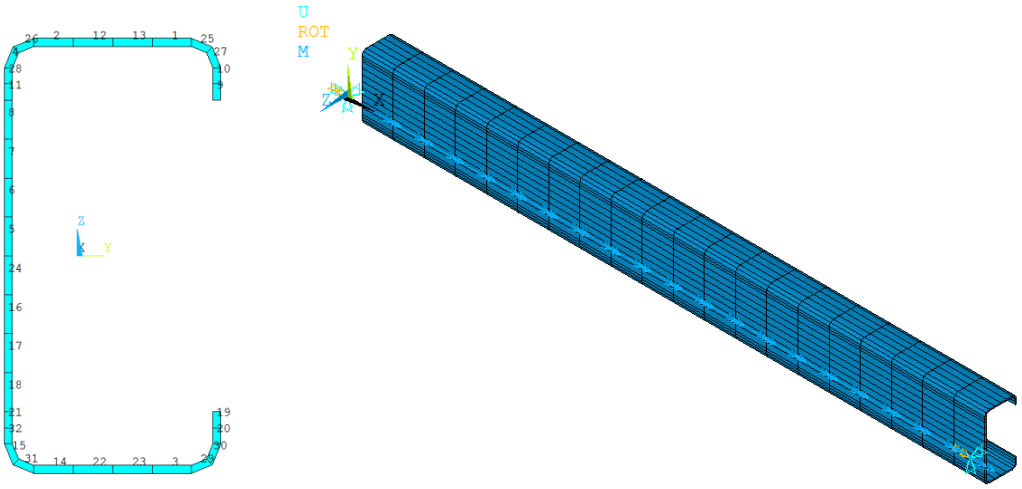

(a) Section cells (b) Beam model

Fig. 8 Finite element model of lipped channel section

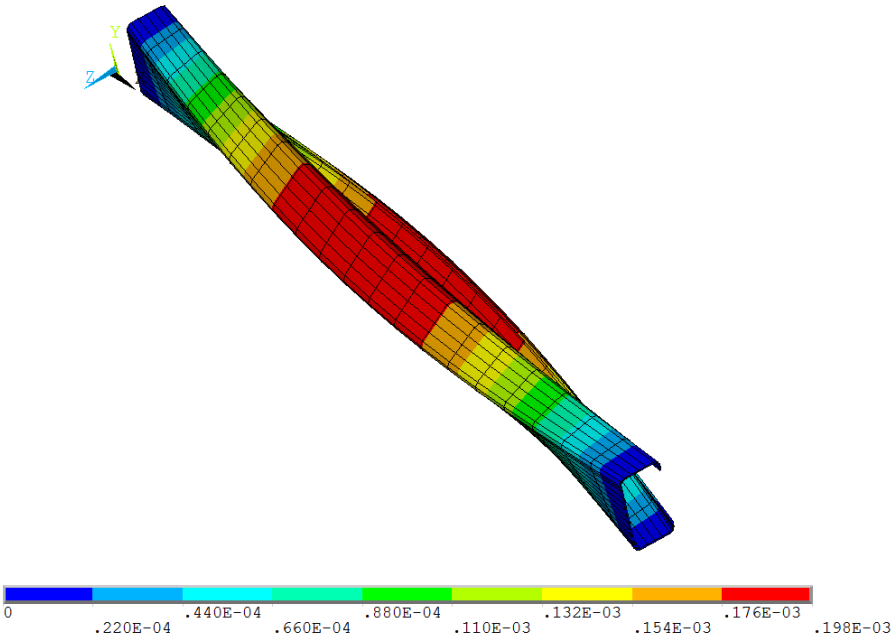

Fig. 9 Twisting of lipped channel section

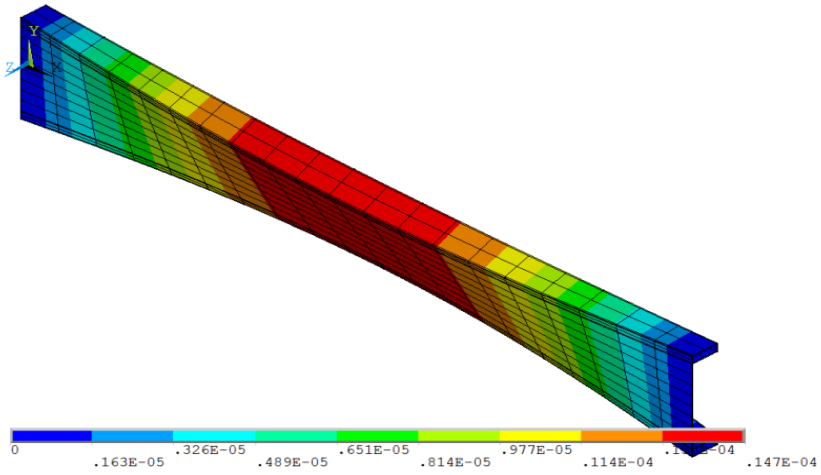

Fig. 10 Twisting of HFC Section 1 with 2m span

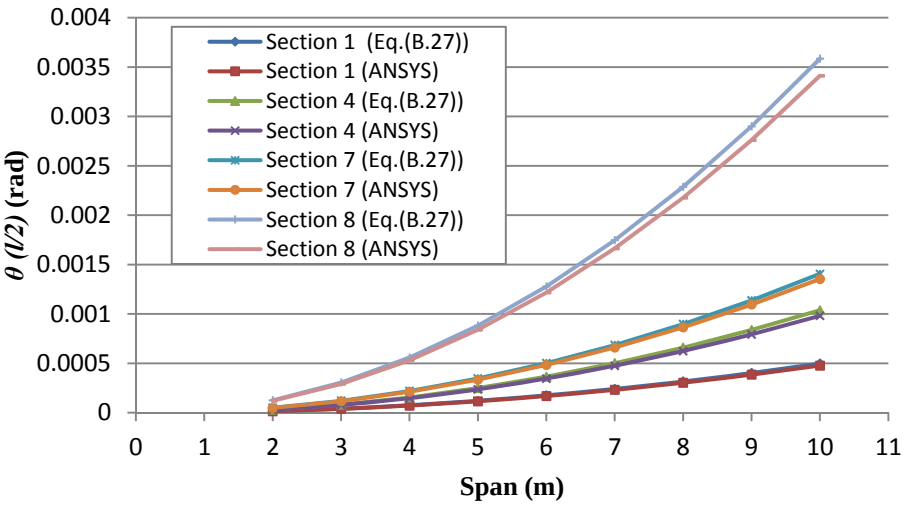

Fig. 11 Comparison of angle of twist at mid-span

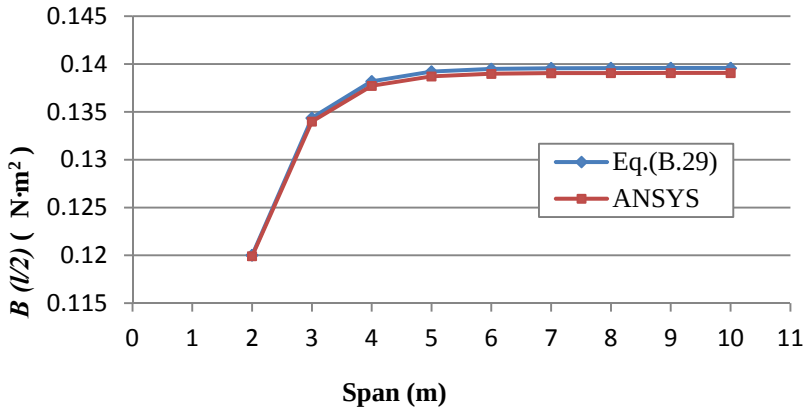

Fig. 12 Comparison of bimoment for HFC Section 1 at mid-span

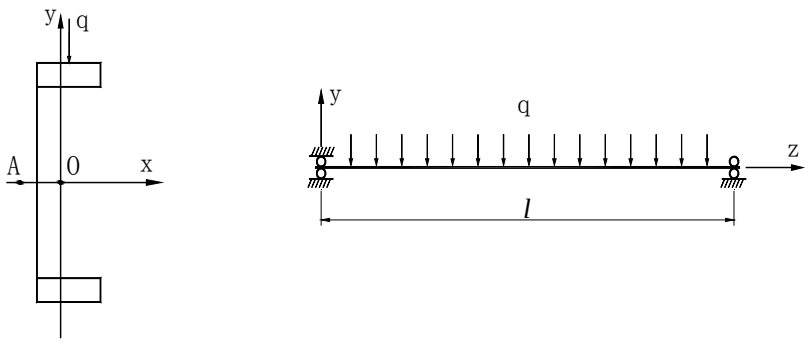

Fig. 13 Transverse load distribution

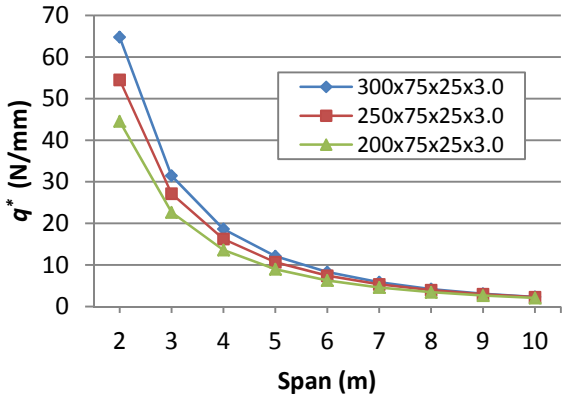

(a) Effect of section depth

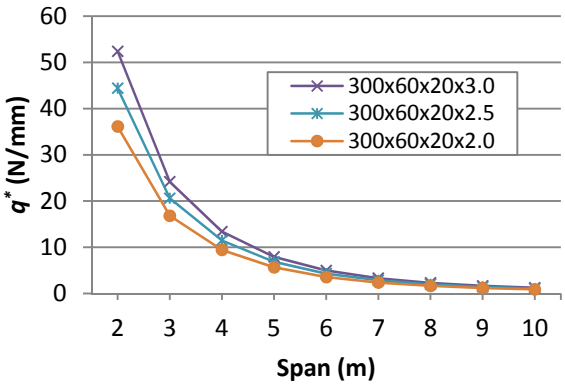

(b) Effect of thickness

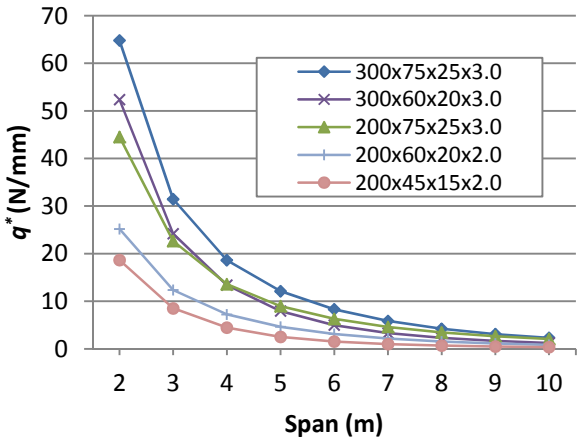

(c) Effect of flange size

Fig. 14 Effects of section parameters on *q

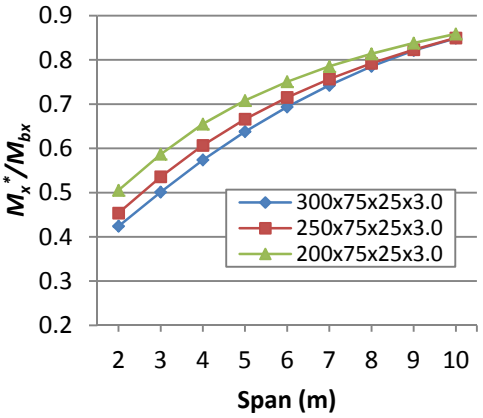

(a) Varying depths

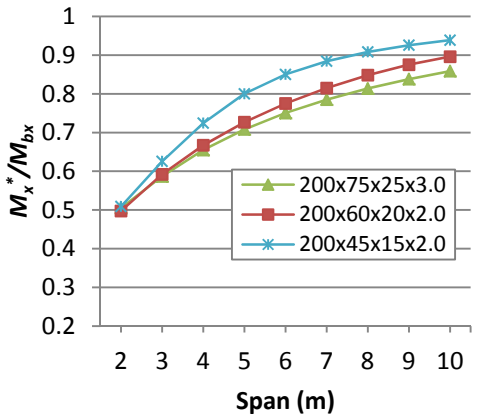

(b) Varying flanges with section depth =200mm

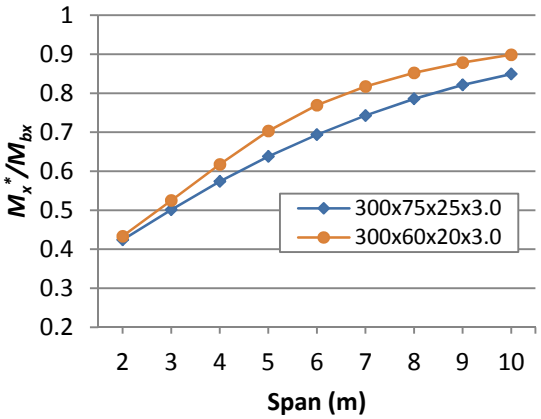

(c) Varying flanges with section depth =300mm

Fig. 15 M_x^*/M_{bx} versus span curves

Table 1 HFC Section dimensions and constants

Section No.	Dimensions (mm) $d^{a,e} \times b_f{}^{b,e} \times d_f{}^{c,e} \times t^d$	Shear centre $x_A(mm)$	Generalized principal fan-shaped area coordinates $\bar{\omega}_1(mm^2)$	$\bar{\omega}_{2,6}(mm^2)$	$\bar{\omega}_3(mm^2)$	$\bar{\omega}_4(mm^2)$	$\bar{\omega}_5(mm^2)$	Principal warping constant $J_{\bar{\omega}}(mm^6)$
1	300×75×25×3.0	-50.4	0	3646.85	3910.37	-4826.91	-6674.42	1.7317E+10
2	250×75×25×3.0	-52.9	0	2994.45	3272.78	-3664.50	-5526.82	1.0999E+10
3	200×75×25×3.0	-55.5	0	2287.53	2574.66	-2562.62	-4433.75	6.3094E+09
4	300×60×20×3.0	-36.9	0	2872.07	3020.76	-4252.14	-5369.82	9.5331E+09
5	300×60×20×2.5	-37.4	0	2898.38	3050.04	-4262.05	-5419.95	8.1735E+09
6	300×60×20×2.0	-37.9	0	2924.35	3078.91	-4271.83	-5470.39	6.7252E+09
7	200×60×20×2.0	-42.7	0	1924.80	2105.27	-2345.47	-3569.94	2.4585E+09
8	200×45×15×2.0	-29.1	0	1453.35	1543.27	-2024.96	-2673.88	1.1485E+09
9	150×45×15×2.0	-31.5	0	1074.80	1174.09	-1319.14	-1977.43	5.6147E+08

[a] d =Section depth; [b] b_f =Flange width; [c] d_f =Flange depth; [d] t =Thickness; [e] d, b_f, d_f =External dimensions

Table 2 Warping factors

Section No.	1	2	3	4	5	6	7	8	9
$J_d(mm^4)$	322582	322132	321682	154631	136372	115429	115162	45099	44965
$J_\rho(mm^4)$	18522031	13044437	8618686	14514865	12230892	9893520	4500929	3257550	1864866
$\nu = 1 - J_d/J_\rho$	0.983	0.975	0.963	0.989	0.989	0.988	0.974	0.986	0.976

Table 3 Dimensions of cold-formed lipped channel sections [25]

Section	Section depth (mm)	Flange width (mm)	Flange depth (mm)	Thickness (mm)	Corner Inside radius (mm)
C10019	102	51	14.5	1.9	5
C10010	102	51	12.5	1.0	5

Table 4 Section properties of cold-formed lipped channel sections

Section		Area	Moment of inertia		Torsion constant	Warping constant
		$A(\text{mm}^2)$	$I_x(\text{mm}^4)$	$I_y(\text{mm}^4)$	$J(\text{mm}^4)$	$I_\omega(\text{mm}^6)$
C10019	Ref.[25]	408.40	671540	141770	491.44	3.1067E+08
	FEA	408.80	673069	142334	499.96	3.1200E+08
C10010	Ref.[25]	215.34	363090	75244	71.78	1.6016E+08
	FEA	215.50	363745	75462	76.27	1.6075E+08

Table 5 Comparison of mid-span twist angle and bimoment

Section	l (mm)	$\theta(l/2)$ (rad)			$B(l/2)$ (Nmm^2)		
		Eq. (37)	FEA	Ratio	Eq. (38)	FEA	Ratio
C10019	1000	1.97E-4	1.98E-4	0.996	1.18E+5	1.18E+5	1.000
	2000	2.69E-3	2.67E-3	1.005	3.98E+5	3.97E+5	1.003
	3000	1.09E-2	1.08E-2	1.008	7.13E+5	7.09E+5	1.005
C10010	1000	3.99E-4	4.01E-4	0.996	1.23E+5	1.23E+5	1.000
	2000	6.08E-3	6.05E-3	1.005	4.66E+5	4.65E+5	1.004
	3000	2.84E-2	2.81E-2	1.011	9.68E5	9.60E+5	1.008

Table 6 Comparison of section constants

Section	$J_d(mm^4)$			$x_A(mm)$			$J_{\bar{\omega}}(mm^6)$		
No.	Eq. (7)	FEA	Ratio	Eq. (24a)	FEA	Ratio	Eq. (12)	FEA	Ratio
1	322582	337250	0.957	-50.4	-50.6	0.996	1.7317E+10	1.8038E+10	0.960
2	322132	336780	0.957	-52.9	-53.1	0.996	1.0999E+10	1.1672E+10	0.942
3	321682	336300	0.957	-55.5	-55.8	0.995	6.3094E+09	6.9069E+09	0.913
4	154631	163540	0.946	-36.9	-37.1	0.995	9.5331E+09	9.7469E+09	0.978
5	136372	142830	0.955	-37.4	-37.6	0.995	8.1735E+09	8.3741E+09	0.976
6	115429	119810	0.963	-37.9	-38.1	0.995	6.7252E+09	6.9062E+09	0.974
7	115162	119540	0.963	-42.7	-42.9	0.995	2.4585E+09	2.6177E+09	0.939
8	45099	47386	0.952	-29.1	-29.2	0.997	1.1485E+09	1.1846E+09	0.970
9	44965	47247	0.952	-31.5	-31.7	0.994	5.6147E+08	5.9457E+08	0.944